WILEY-VCH

DOI: 10.1002/((please add manuscript number))
Article type: Communication

Molecular Transport Junctions Created By Self-Contacting Gapped Nanowires

Jong Kuk Lim,[1] One-Sun Lee,[4] Jae-Won Jang,[5] Sarah Hurst Petrosko,[2,3] George C. Schatz,[2,6] and Chad A. Mirkin[2,3,7]**

Prof. Jong Kuk Lim
Department of Chemistry, Chosun University
Gwangju 501-759, Korea
E-mail: jklim@chosun.ac.kr

Dr. Sarah Hurst Petrosko, Prof. George C. Schatz, Prof. Chad A. Mirkin
Department of Chemistry and International Institute for Nanotechnology, Northwestern University
2145 Sheridan Road, Evanston, Illinois 60208, USA
E-mail: chadnano@northwestern.edu

Dr. One-Sun Lee
Qatar Environment and Energy Research Institute, Hamad Bin Khalifa University,
Qatar Foundation, P.O. Box 5825, Doha, Qatar

Prof. Jae-Won Jang
Department of Physics, Pukyong National University
Busan 608-737, Korea

Keywords: molecular transport junction, on-wire lithography, molecular electronics, DLVO theory

To realize the promise of molecular electronic devices, methods must be developed for creating molecular transport junctions (MTJs), tiny gaps between electrodes connected with molecules, in a straightforward and reproducible fashion.[1] Many approaches to synthesize MTJs have been proposed, based on nanopores,[2] scanning probes,[3] liquid metals,[4] wire crossings,[5,6] electromigration,[7] break junctions,[8] on-edge junctions,[9] cross bars,[10] and on-wire lithography (OWL).[11–13] OWL is a particularly attractive method for fabricating MTJs because it can be used to rapidly and routinely create

sub-5 nm gaps along the long axis of the wire in a high-throughput fashion. In addition, OWL and related techniques (i.e., co-axial lithography (COAL) provide precise architectural control of the dimensions and elemental composition of nanostructures in both the axial and radial directions.

In a typical OWL process, metals are deposited electrochemically within the pores of anodic aluminum oxide (AAO) templates, and different metals can be sequentially deposited by changing the electrolyte solution used to make striped nanowires. The segment length can be tuned by varying the electric charge that is passed during the electrodeposition process.[14] These segmented nanowires are removed from the template by dissolving the AAO, and then drop-coated on glass slides for further deposition of a backing layer (e.g., silica or silver). Once a backing layer is formed on the segmented nanowires, the sacrificial metal segments can be selectively removed from the nanowires via chemical etching steps. Because the backing layer holds the segments in place, the gaps between the segments are maintained, and tiny spaces are created that can be spanned by molecules.

OWL-based nanowires have been successfully used to prepare MTJs in the past.[11-13] Specifically, molecular rectifiers were prepared using two different metals on opposing sides of the nanogap. Specially designed molecules (~3 nm in length) trapped therein successfully showed rectifier properties.[15] In addition, when the metal segments in the MTJs are composed of a noble metal, such as Au, the strong electromagnetic field in the nanogap led to enhancements in the intensity of the Raman signals of the molecules localized within them.[16] This property has been used for biological detection[17] and the creation of other novel encoding strategies.[18]

However, the fabrication of MTJs containing molecules shorter than 2 nm still remains a considerable challenge, even using techniques like OWL.[11-13] Herein, we introduce a new OWL-related method in which segmented nanowires with ~10 nm gaps are used to fabricate MTJs. After molecules are adsorbed into the gap, MTJs are subsequently formed by capillary or van der Waals forces. The gap size is adjusted to match the molecular length, and therefore one batch of segmented nanowires can be

used to investigate molecules of different lengths, especially those less than 2 nm in length. As a proof-of-concept, we fabricated MTJs using two different molecules (1,6-hexane dithiol, and 1,3-diethynyl benzene) employing this method.

We first chose to analyze the contact behavior of a relatively simple system, without molecules, to fully understand the fundamental science involved from both experimental and theoretical standpoints. Au-Ni-Au segmented nanowires were prepared via OWL with segment lengths of ~1.5 μm (Au), ~40 nm (Ni), and ~1.5 μm (Au) (see Figures 1a and 1b).[14] In a typical experiment, the as-prepared Au-Ni-Au segmented nanowires were placed onto silicon substrates, and the Ni segments were selectively removed using 50% aqueous HCl. The etching solution was then exchanged for deionized (DI) water, and the Au segments came into contact as the solution slowly evaporated (over several to tens of hours, system was covered) (Figure 1c). This is termed a "self-contacting" method because mechanical force is not applied to make the two segments come into contact with each other Note that the two Au segments came in contact with each other over only small cross-sectional areas because these surfaces are not atomically flat (confirmed using transmission electron microscopy (TEM)) (Figure 1d).[19]

To explore the conductivity of the as-prepared nanowires, two-terminal *I-V* experiments were performed at room temperature. The nanowires were connected by electron-beam lithography (EBL) to larger Au electrodes pre-patterned onto Si wafers using previously reported photolithographic strategies (Figure 1e).[11-13] These devices showed linear Ohmic behavior with a resistivity of 7.9×10^{-6} Ω·m (blue trace in Figure 1e), which is similar to the resistivity of a pure Au nanowire (6.7×10^{-6} Ω·m, red trace in Figure 1e). Of the tested wires, 92% (11 out of the 12 tested wires) showed metallic Ohmic behavior, which indicates that contact was successfully made between the two gold segments allowing electric current to pass, and a significant oxide layer was not formed on the cross-sectional surfaces of the Au segments. In general, as the thickness of the oxide film gets larger, the contact junctions between metals become more insulating.[20]

To understand the physics of junction formation, we note that capillary ($F_{capillary}$) and van der Waals (F_{vdW}) forces are expected to be the dominant attractive forces, while electric double layer (F_{EDL}) and friction ($F_{friction}$) forces are important repulsive forces (of course Pauli repulsion takes over at very short range).[21] Here we will calculate and compare the magnitude of each force to understand the main driving forces for the self-contacting behavior. When the two Au segments are separated by relatively large distances (> 10 nm), they can be brought near each other by the $F_{capillary}$ of the evaporating water. When the cross-sectional surfaces of the Au segments are not passivated by molecules, $F_{capillary}$ mainly acts between the two cross-sectional walls of the Au segments (Figure 2a). Let us consider two segments separated by a distance D. The force $F_{capillary}$, which contributes to bringing the two segments together, can be calculated from Equation (1) (derived in the Supporting Information):[22,23]

$$F_{capillary}(D) = \frac{2\pi R_{nanowire}^2 \gamma \cos\theta}{D} \quad (1)$$

where $R_{nanowire}$, γ, and θ are the radius of the Au nanowire (180 nm), the surface tension of water (72 mN·m^{-1}), and the water contact angle (64°) on the Au surfaces, respectively.[24] Equation (1) indicates that $F_{capillary}$ varies inversely with D and has a value of 160 nN at a 40 nm separation (red curve in Figure 2b).

F_{vdW} can be calculated using pairwise summation, as described by Hamaker theory.[22,25] This shows that the F_{vdW} acting on two nanowires with the same length L and radius $R_{nanowire}$, varies with D according to Equation (2)[25] (black curve in Figure 2b),

$$F_{vdW}(D) = \frac{A}{5} R_{nanowire}^4 \left[\frac{1}{D^5} - \frac{2}{(D+L)^5} + \frac{1}{(D+2L)^5} \right] \quad (2)$$

where A is the Hamaker constant (40 × 10^{-20} J for Au in water).[22] According to Equation (2), F_{vdW} increases as the inverse-fifth power of distance D for small values of D (< 10 nm). At an initial separation of 40 nm, F_{vdW} is 0.8 nN, which is smaller than $F_{capillary}$. When the distance between the two

Au segments decreases as a result of $F_{capillary}$, F_{vdW} reaches 628 nN at a D of 10.6 nm and begins to dominate $F_{capillary}$. The total attractive forces acting between the two Au segments are obtained by adding $F_{capillary}$ and F_{vdW} (blue curve in Figure 2b). As expected, $F_{capillary}$ is dominant at longer distances (≥ ~10 nm), and F_{vdW} is dominant at shorter distances (≤ ~10 nm).

For self-contact to be induced by these attractive interactions, the total attractive forces must overcome the two dominant types of repulsive forces: (1) electric double layer (EDL) repulsive forces, F_{EDL},[22] and (2) frictional forces, $F_{friction}$. Because the two Au segments are brought into contact with each other in solution, the surfaces of the two Au segments will be covered by EDLs composed of ions, which cause the surfaces to repel one another. Although these experiments are performed in DI water, the pH of pure water exposed to air is slightly acidic (~5.7) because of dissolved CO_2. F_{EDL} can be expressed as a function of distance D as follows:[22]

$$F_{EDL}(D) = \pi R_{nanowire}^2 \times 0.0482[H_2CO_3]^{\frac{1}{2}} \tanh^2[\frac{\psi_0}{103}]e^{-\kappa D} \bullet (-\kappa) \quad (3)$$

where $[H_2CO_3]$ is the molar concentration of H_2CO_3, ψ_0 is the surface potential in meV, κ is the inverse Debye length, and F_{EDL} is expressed in newtons. At pH 5.7, the concentration of H_2CO_3 was calculated to be 1.7×10^{-5} M. The zeta potential (−18 mV) measured for Au discs (diameter: 360 nm, thickness: 250 nm) was used for the surface potential (ψ_0). The value of κ was calculated from the $[H_2CO_3]$ by using Equation (4).[22] As a result of these calculations, it is apparent that, for this system, F_{EDL} (a repulsive force) is smaller (~10^{-12} N) than the net attractive forces (~10^{-7} N) by five orders of magnitude. Therefore, we will not consider F_{EDL} in calculating the total repulsive forces.

$$\kappa = \frac{\sqrt{[H_2CO_3]}}{0.304} = 0.01355 \text{ nm}^{-1} \quad (4)$$

The frictional force of the nanowire ($F_{friction}$) at the nanoscale is proportional to the total area of the contact region ($A_{nanowire}$) between the substrate and the nanowires (Figure 2c).[26,27] If we know the

mathematical function relating $F_{friction}$ and $A_{nanowire}$, and the dimensions of the contact region—its width ($d_{nanowire,contact}$) and total active length ($l_{active,total}$)—, $F_{friction}$ can be easily obtained by calculating $A_{nanowire}$ ($A_{nanowire} = 2d_{nanowire,contact} \times l_{active,total}$) and applying a known function to it. Unfortunately, that mathematical function is not known, and it is difficult to directly measure the dimensions of the contact region, $d_{nanowire,contact}$ and $l_{active,total}$. Thus, we will use experimental data previously reported in the literature[27] to obtain $d_{nanowire,contact}$. We can calculate $A_{nanowire}$ as a function of $l_{active,total}$, and estimate $F_{friction}$ by comparing $A_{nanowire}$ to those reported values as follows.[28] When a nanowire with radius $R_{nanowire}$ contacts a plane with adhesion energy per unit area, $W_{nanowire}$, the width of contact region for the nanowire ($d_{nanowire,contact}$) at zero normal force is given by the Derjaguin–Muller–Toporov model[29] (Equation 5):

$$\mathrm{d}_{\mathrm{nanowire,contact}} = 2 \times \left(\frac{2\pi R_{\mathrm{nanowire}}^2 \mathrm{W}_{\mathrm{nanowire}}}{\mathrm{K}} \right)^{\frac{1}{3}} \quad (5)$$

where K is the reduced elastic modulus, obtained from both the Young's modulus and the Poisson's ratio of the two contacting materials (see the Supporting Information). Directly measuring the adhesion energy per unit area of nanowire ($W_{nanowire}$) is difficult; therefore, we used the value (0.073 $J \cdot m^{-2}$) reported in a previous study,[27] where the authors obtained the adhesion energy per unit area (W_{tip}) between silicon nitride (Si_3N_4) atomic force microscopy (AFM) tips with a radius of 50 nm and *n*-octadecanethiol monolayers assembled on Au surfaces. It can be assumed that the two contacting materials (Si_3N_4, and the *n*-octadecanethiol monolayer assembled on Au surfaces) used in that study are similar to the ones used in our experiment (Si and a 1-dodecanethiol monolayer passivated on Au nanowires) because the chemical structure of *n*-octadecanethiol is similar to 1-dodecanethiol and both the Young's modulus (140 GPa) and the Poisson's ratio (0.3) of Si_3N_4 are similar to those of Si (160 GPa and 0.27, respectively).[28,30] Under the assumption that W_{tip} is similar to $W_{nanowire}$, the contact

region width for the nanowire ($d_{nanowire,contact}$) was calculated to be 5.7 nm (see the Supporting Information). Finally, the area of the contact region for the nanowire ($A_{nanowire,contact}$) can be expressed as a function of $l_{active,total}$ as follows:

$$A_{nanowire,contact} = 2d_{nanowire,contact} \times l_{active,total} = 11.4 \text{ nm} \times l_{active,total} \quad (6)$$

We should note that $l_{active,total}$ is different from the total length of the nanowire (1.5 μm) because the two surfaces contact the substrate only at the summits of a large number of asperities on the surfaces, as a consequence of the nanoscopic roughness of the surfaces.[31,32] Using the same logic, the area of the contact region ($A_{tip,contact}$) between the Si_3N_4 AFM tip and the *n*-octadecanethiol monolayers assembled on Au surfaces was calculated to be 1.8×10^{-17} m^2. The measured frictional force for the Si_3N_4 AFM tip ($F_{friction,tip}$) on the *n*-octadecanethiol monolayers assembled on Au surfaces was 0.5 nN;[28] hence, $F_{friction}$ can be predicted using Equation (7) (see Supporting Information).

$$F_{friction,nanowire} = 0.5 \text{ nN} \times \frac{A_{nanowire,contact}}{A_{tip,contact}} \quad (7)$$

Finally, $F_{friction}$ is expressed as a linear function of $l_{active,total}$.

$$F_{friction,nanowire}\left(\text{nN}\right) = 3.2 \times 10^{-1}\left(\frac{\text{nN}}{\text{nm}}\right) \times l_{active,total}\left(\text{nm}\right) \quad (8)$$

When $l_{active,total}$ is ~500 nm, $F_{friction}$ is balanced by the total attractive forces (dashed line in Figure 2b). This means that if $l_{active,total}$ is larger than ~500 nm, the frictional force is stronger than the total attractive forces ($F_{capillary} + F_{vdW}$) and the two Au segments will not move. On the other hand, if $l_{active,total}$ is smaller than ~500 nm, the two Au segments can move and form junctions (Figure 1e). Because it was observed that a high percentage of metallic Ohmic contact junctions were formed (Figure 1), we expect $l_{active,total}$ to have been less than ~500 nm for most of the nanowires used in this experiment. In addition to $l_{active,total}$, the nanowire diameter ($R_{nanowire}$) is also an important factor in determining the occurrence of self-contact because $F_{capillary}$, F_{vdW}, and $F_{friction,nanowire}$ vary with $R_{nanowire}$. While $F_{capillary}$ and F_{vdW} are

proportional to the square and fourth power of $R_{nanowire}$, respectively, $F_{friction,nanowire}$ increases with the two-thirds power of $R_{nanowire}$ (Equations 1, 2, and 5). For the variation of $R_{nanowire}$ commencing at a separation of 40 nm, $F_{friction}$ was only compared to $F_{capillary}$ because at these values of separation F_{vdW} is much smaller than the other two forces. With fixed $l_{active,total}$ (~500 nm), $F_{capillary}$ and $F_{friction}$ were calculated and plotted against $R_{nanowire}$ (see Supporting Information). When $R_{nanowire} < \sim 180$ nm, $F_{friction}$ is stronger than $F_{capillary}$. On the contrary, $F_{capillary}$ is stronger than $F_{friction}$ when $R_{nanowire} > \sim 180$ nm. With these calculations and experimental results, we predict that this self-contacting process can be used to develop MTJs if molecules are assembled at the cross-sectional surfaces of the Au segments before self-contact between the Au segments occurs.

Armed with these experimental and theoretical investigations, we fabricated MTJs using the self-contacting approach outlined in Scheme 1. We prepared 360-nm diameter wires comprised of gold segments (1.5 μm long) separated by Ni (20 nm) and Ag (20 nm) spacer layers adhered to a silver backing layer (Scheme 1). These structures were passivated with 1-dodecanethiol (1-DDT), which was adsorbed onto the exposed Au segments. The Ni segment was chemically dissolved with 50% HCl, forming a gap in the structure and exposing the end of one of the gold segments. Then, we added either 1,4-diethynyl benzene (1,4-DEB; left route of Scheme 1) or 1,6-hexane dithiol (1,6-HDT) as described in Scheme 1b and 1c), and these molecules were adsorbed onto the end of the exposed gold segments. (Note that there could be some exchange of these molecules with those of the 1-DDT passivating layer, but this will not affect the MTJ measurements). We then etched the silver backing layer and the silver spacer segment with MeOH:NH_4OH:H_2O_2 (4:1:1, v/v), creating a structure where the molecule of interest exists in the gap, but does not yet bridge it because of the much larger gap size. Next, the etching solution was exchanged with deionized (DI) water, and this water was allowed to slowly evaporate. A combination of capillary and van der Waals forces drove the two segments together, allowing the molecules to link them and thus creating a functional MTJ.

The *I-V* characteristics of the junctions prepared with 1,4-diethynyl benzene (1,4-DEB) as the bridging molecule were measured under ambient conditions (black line in Figure 3a, 3c, and 3e). In this experiment, 1,4-DEB was selected as the test molecule, because it easily adsorbs onto the Au surface.[33,34] As a control experiment, the conductivities of the self-contacting junctions with the 1,4-DEB bridge were compared with those bridged by a poorly conducting molecule, 1,6-hexanedithiol (1,6-HDT) (black line in Figures 3b, 3d, and 3f) with a similar length (1 nm). From the shape of the *I-V* curve we can observe that the contact for both molecular junctions shows a behavior that is in-between Ohmic and insulating (i.e., semiconducting). None of the devices formed in the absence of molecules (11 out of 12 tested wires, Figure 1) showed semiconducting properties, suggesting that the semiconducting layer formed at the junctions is due to the presence of the 1,4-DEB molecules. Moreover, the conductivity of the 1,4-DEB-functionalized wires is ~10,000 times larger than that of 1,6-HDT-functionalized wires. The current for the 1,4-DEB contained in the MTJ devices is on average a few μA (Figure 3a); on the other hand, for 1,6-HDT, only currents in the pA range were observed (Figure 3b). Because the conductivities through both molecules were measured at the same gap distance (1 nm), the gap distance effect can be excluded as a contributing factor to the different observed conductivities. As a result, we conclude that the resulting *I-V* curves indicate the presence of molecules at the junctions.

To verify that the semiconducting behavior of the junctions is due to the molecular bridges rather than by water condensed at the junctions (under ambient conditions, water is easily condensed at the nano-asperities of these junctions), *I-V* curves were measured for the devices containing 1,4-DEB, and 1,6-HDT in vacuum (6×10^{-6} Torr). In vacuum, all water condensed at the junctions evaporates. Significantly, the *I-V* profile in vacuum (red line of Figure 3a and 3b) is almost the same as that taken under ambient conditions, indicating that the measured currents at the junctions under ambient conditions result from the adsorbed molecules, not from water (black line of Figure 3a and 3b).

In summary, we have demonstrated that MTJs can be fabricated by bringing segments of nanowires into contact via capillary forces, taking advantage of $F_{capillary}$ and F_{vdW}. We further show that the combination of $F_{capillary}$ and F_{vdW} can overcome the repulsive forces of F_{EDL} and $F_{friction}$ when the total active length, $l_{active,total}$, of each Au segment is below ~500 nm, and the radius of each Au segment, $R_{nanowire}$, is larger than ~180 nm. This method may become a widely adopted and convenient technique for preparing MTJs bridged with molecules, especially for those structures below 2 nm in length, which are challenging to fabricate via traditional MTJ preparation techniques.

Experimental Section

Preparation of nanowires: In a typical experiment, 360-nm-diameter segmented nanowires were synthesized, according to literature methods.[14] Ag was thermally evaporated onto the back of an anodic aluminum oxide (AAO) template (Whatman). The silver-coated alumina template was placed (silver side down) in an electrochemical cell containing a Pt counter electrode and an Ag/AgCl reference electrode. Electrolyte solutions used for Ag, Ni, and Au segment deposition were 1025 RTU, Nickel Sulfamate SEMI Bright RTU, and Orotemp 24 RTU (Technic, Inc.), respectively. After the electrodeposition of the segmented nanowires was completed, the template was placed in concentrated nitric acid for 15 min to remove the silver backing layer, and then rinsed with water and placed in a 3 M sodium hydroxide solution for 2 h, to dissolve the AAO template. The nanowires were repeatedly rinsed with distilled water until the pH of the rinsing solution remained at 7. For making Ag backing layers as in Scheme 1, as-prepared segmented nanowires were spread onto glass slides and 50 nm of Ag was thermally evaporated. The nanowires were released from the glass slides into an isopropyl alcohol (IPA) solution containing excess 1-dodecanethiol by sonication.

Preparation of self-contacting junctions: The surfaces of the nanowires released from the glass slides were passivated with 1-dodecanethiol. Passivated nanowires were spread onto silicon wafers for SEM analysis or onto the carbon films of grids for TEM analysis. The substrates or grids were immersed in Ni

etchants (HCl 1% v/v, aq.), and the Ni etchant was diluted with water until the pH of the rinsing solution remained at 7. The rinsing solvent was exchanged with ethanol containing 1,4-diethynyl benzene (1,4-DEB) or 1,6-hexane dithiol (1,6-HDT). After 14 h, the Ag backing layers and segments were removed in Ag etchant ($MeOH:NH_4OH:H_2O_2$, 4:1:1, v/v) for ~2 h, and the Ag etchant was then exchanged with DI water. The segmented nanowires on the substrates or grids were then allowed to dry, which resulted in the formation of MTJs via self-contact.

Microscopy: The morphologies of the nanowires were characterized with a scanning electron microscope (Gemini 1525, LEO) and a transmission electron microscope (H8100, Hitachi). An inverted fluorescence optical microscope (Axiovert 200MAT, ZEISS) or a confocal Raman microscope (CRM200, WITec) was used for observing fluorescein and methylene blue (Figure S2, Supporting Information).

Selective adsorption of molecules onto the cross-sectional surfaces of the Au segments: In a typical experiment, the Au outer surfaces of the Au-Ni-Au segments were first passivated with 1-dodecanethiol, and the Ni segments were then removed by exposure to the etching solution. After the etching solution was neutralized, fluorescein or methylene blue (MB) was adsorbed onto the cross-sectional Au surfaces for 12 h or 60 h, respectively, and the fluorescence or Raman signals of the dye on the nanowires were observed using fluorescence optical microscopy or confocal Raman scanning optical microscopy (Figure S2). The intensities of the fluorescence and Raman signals are the strongest at the nanowire junctions. From these images, it can be concluded that the fluorescein or MB was adsorbed primarily at the end of the Au segment that forms the inner side of the junction. In the case of MB, a strong Raman signal at the junction can also result from the enhanced electromagnetic field effect at the junction.[16] It has been reported that the electromagnetic enhancement factor (EF) at the junction between segments oscillates as a function of the segment length, and that the EF at the junction between 1.44 μm-long Au segments is a minimum.[34] We can therefore conclude that the surface enhanced Raman scattering (SERS) effect is

weak when the segment length is 1.5 μm, and it is not the cause of the strong Raman signal in the gap. Rather, the Raman signal occurs with a large signal-to-noise ratio in the gap because the dye molecules are assembled primarily in the gap and not on the external surfaces.

Electronic addressability and measurement: One drop of an isopropyl alcohol suspension of nanowires was drop-cast on a substrate prefabricated with photolithographic patterns, and the solvent was then allowed to evaporate. Polymethylmethacrylate (PMMA) was coated on the surfaces of patterns where nanowires were already spread, and electron beam lithography (EBL) was performed using a FEI Quanta field emission scanning electron microscope (Electron Probe Instrumentation Center (EPIC), NUANCE, Northwestern University) equipped with the Nabity Pattern Generation System (NPGS, JC Nabity Lithography System) at a 30-kV acceleration voltage. The EBL-patterned substrates were developed with 3:1 (v/v) isopropyl alcohol (IPA)/methyl isobutyl ketone(MIBK) solution for 30 s, rinsed with IPA for 10 s, and then rinsed with water. After defining the inner electrode patterns on the substrates using EBL, Cr (10 nm) and Au (450 nm) were thermally evaporated onto the patterned substrates. Finally, the PMMA was removed in acetone (i.e., a lift-off procedure). The self-contacting MTJs were connected to the Au microelectrodes by EBL, under the conditions described above. Electronic measurements were carried out with a probe station (S-1160, Signatone Corp.). Current-voltage measurements (Model 6430, Keithley Instruments Inc.) were taken under either ambient or vacuum (6×10^{-6} Torr) conditions.

Supporting Information

Supporting Information is available from the Wiley Online Library or from the author.

Acknowledgements

This material is based upon work supported as part of the Non-Equilibrium Energy Research Center (NERC), an Energy Frontier Research Center funded by the U.S. Department of Energy, Office of Science, Office of Basic Energy Sciences under Award Number DE-SC0000989, the Department of the Navy, Office of Naval Research (N00014-11-1-0729), NSF Grant CHE-1147335, and the Nanoscale

Science and Engineering Initiative of the National Science Foundation under NSF Award No. EEC-0647560. This material is also based upon work supported by the DoD/NSSEFF Program/Naval Postgraduate School under Award No. N00244-09-1-0012 and N00244-09-1-0071. We thank Profs. Adam B. Braunschweig and Wooyoung Shim for assistance in preparing this manuscript.

Received: ((will be filled in by the editorial staff))
Revised: ((will be filled in by the editorial staff))
Published online: ((will be filled in by the editorial staff))

[1] R. L. McCreery, A. J. Bergren, *Adv. Mater.* **2009**, *21*, 1.

[2] J. Chen, M. A. Reed, A. M. Rawlett, J. M. Tour, *Science* **1999**, *286*, 1550.

[3] B. Xu, N. J. Tao, *Science* **2003**, *301*, 1221.

[4] R. E. Holmlin, R. Haag, M. L. Chabinyc, R. F. Ismagilov, A. E. Cohen, A. terfort, M. A. Rampi, G. M. Whitesides, *J. Am. Chem. Soc.* **2001**, *123*, 5075.

[5] J. G. Kushmerick, D. B. Holt, S. K. Pollack, M. A. Ratner, J. C. Yang, T. L. Schull, J. Naciri, M. H. Moore, R. Shashidhar, *J. Am. Chem. Soc.* **2002**, *124*, 10654.

[6] J. E. Green, J. W. Choi, A. Boukai, Y. Bunimovich, E. J.-Halperin, E. Delonno, Y. Luo, B. A. Sheriff, K. Xu, Y. S. Shin, H.-R. Tseng, F. Stoddart, J. R. Heath, *Nature* **2007**, *445*, 414.

[7] H. Park, A. K. L. Lim, A. P. Alivisatos, J. Park, P. L. McEuen, *Appl. Phys. Lett*. **1999**, *75*. 301.

[8] M. A. Reed, C. Zhou, C. J. Muller, T. P. Burgin, J. M. Tour, *Science* **1997**, *278*, 252.

[9] T. Shamai, A. Ophir, Y. Selzer, *Appl. Phys. Lett*. **2007**, *91*, 1021081.

[10] E. D. Mentovich, I. Kalifa, A. Tsukernik. A. Caster, N. Rosenberg-Shraga, H. Marom, M. Gozin, S. Richter, *Small* **2008**, *4*, 55.

[11] X. Chen, Y.-M. Jeon, J.-W. Jang, L. Qin, F. Huo, W. Wei, C. A. Mirkin, *J. Am. Chem. Soc*. **2008**, *130*, 8166.

[12] X. Chen, A. B. Braunschweig, M. J. Wiester, S. Yeganeh, M. A. Ratner, C. A. Mirkin, *Angew. Chem. Int. Ed*. **2009**, *48*, 5178.

[13] A. B. Braunschweig, A. L. Schmucker, W. D. Wei, C. A. Mirkin, *Chem. Phys. Lett*. **2010**, *486*, 89.

[14] L. Qin, S. Park, L. Huang, C. A. Mirkin, *Science* **2005**, *309*, 113.

[15] X. Chen, S. Yeganeh, L. Qin, S. Li, C. Xue, A. B. Braunschweig, G. C. Schatz, M. A. Ratner, C. A. Mirkin, *Nano Lett*. **2009**, *9*, 3974.

[16] L. Qin, S. Zou, C. Xue, A. Atkinson, G. C. Schatz, C. A. Mirkin, *Proc. Nat. Acad. Sci. U.S.A.* **2006**, *103*, 13300.

[17] G. Zheng, L. Qin, C. A. Mirkin, *Angew. Chem. Int. Ed*. **2008**, *47*, 1938.

[18] L. Qin, M. J. Banholzer, J. E. Millstone, C. A. Mirkin, *Nano Lett*. **2007**, *7*, 3849.

[19] M. J. Banholzer, S. Li, J. B. Ketter, D. I. Rozkiewicz, G. C. Schata, C. A. Mirkin, *J. Phys. Chem*. *C* **2008**, *112*, 15729.

[20] R. Holm, *Electric Contacts*, Springer-Verlag GmbH, Heidelberg, Germany **1967**, Pt. 1.

[21] E.-S. Yoon, S. H. Yang, H.-G. Han, H. Kong, *Wear* **2003**, *254*, 974.

[22] J. N. Israelachvili, *Intermolecular and Surface Forces*, Academic Press, Waltham, MA, USA **1991**, Ch. 13.

[23] Hans-Jűrgen Butt, Michael Kappl, *Advances in Colloid and Interface Science* **2008**, *146*, 48.

[24] S. Liu, J. B.-H. Tok, J. Locklin, Z. Bao, *Small* **2006**, *2*, 1448.

[25] V. A. Parsegian, *Van der Waals Forces*, Cambridge University Press, Cambridge, UK **2006**.

[26] L. Sirghi, *Appl. Phys. Lett*. **2003**, *82*, 3755.

[27] M. Enachescu, R. J. A. van den Oetelaar, R. W. Carpick, D. F. Ogletree, C. F. J. Flipse, M. Salmeron, *Tribol. Lett*. **1999**, *7*, 73.

[28] A. Lio, C. Morant, D. F. Ogletree, M. Salmeron*, J. Phys. Chem. B* **1997**, *101*, 4767.

[29] R. W. Carpick, D. F. Ogletree, M. Salmeron, *J. Colloid Interf. Sci*. **1999**, *211*, 395.

[30] P. Hess, *Appl. Surf. Sci* **1996**, *106*, 429.

[31] M. Nosonovsky, B. Bhushan, *Mater. Sci. Eng. R* **2007**, *58*, 162.

[32] B. Bhushan, C. Dandavate, *J. Appl. Phys*. **2000**, *87*, 1201.

[32] J. K. Lim, S.-W. Joo, K. S. Shin, *Vib. Spectrosc.* **2007**, *43*, 330.

[33] S. W. Joo, S. W. Han, K. Kim, *J. Colloid Interf. Sci*. **2001**, *240*, 391.

[34] María L. Pedano, Shuzhou Li, George C. Schatz, Chad A. Mirkin, *Angew. Chem. Int. Ed*. **2010**, *49*, 78.

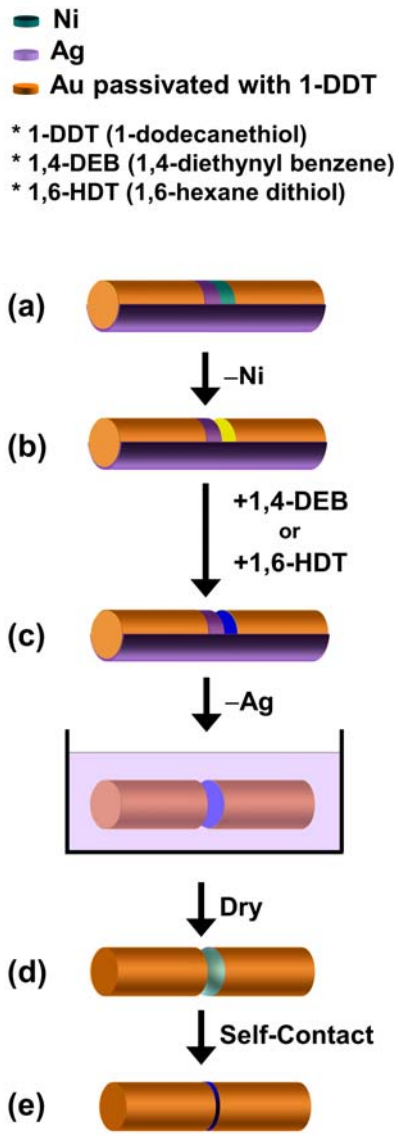

Scheme 1. Fabrication of molecular transport junctions. (a) Au-Ni-Ag-Au segmented nanowires passivated with 1-dodecanethiol were prepared. (b) After removing the Ni segments, (c) 1,4-diethynyl benzene or 1,6-hexanedithiol was adsorbed onto the exposed Au segment surface. (d) Ag segments and backing layers were removed in an Ag etching solution and allowed to dry. (e) Separated Au segments form self-contacting junctions.

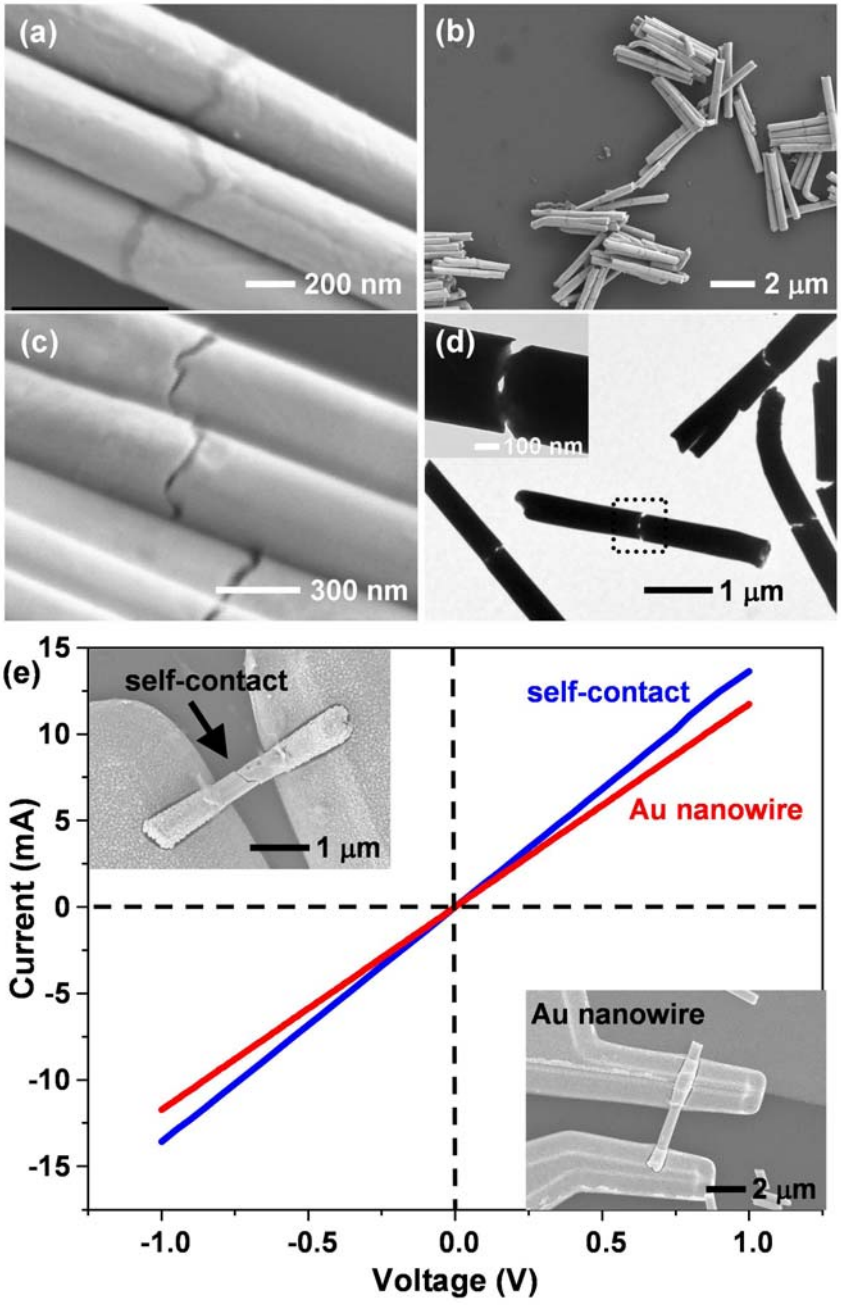

Figure 1. (a), (b) Scanning electron microscope (SEM) images of Au-Ni-Au segmented nanowires with segment lengths of ~1.5 μm for Au and ~40 nm for Ni. (c) SEM image of self-contacting junctions after removing the Ni segments. (d) TEM image of two Au segments in partial contact with each other at the junction interface. (e) The self-contacting junction (upper left inlet) and fully formed Au nanowires (lower right inlet) display comparable electron transport behavior.

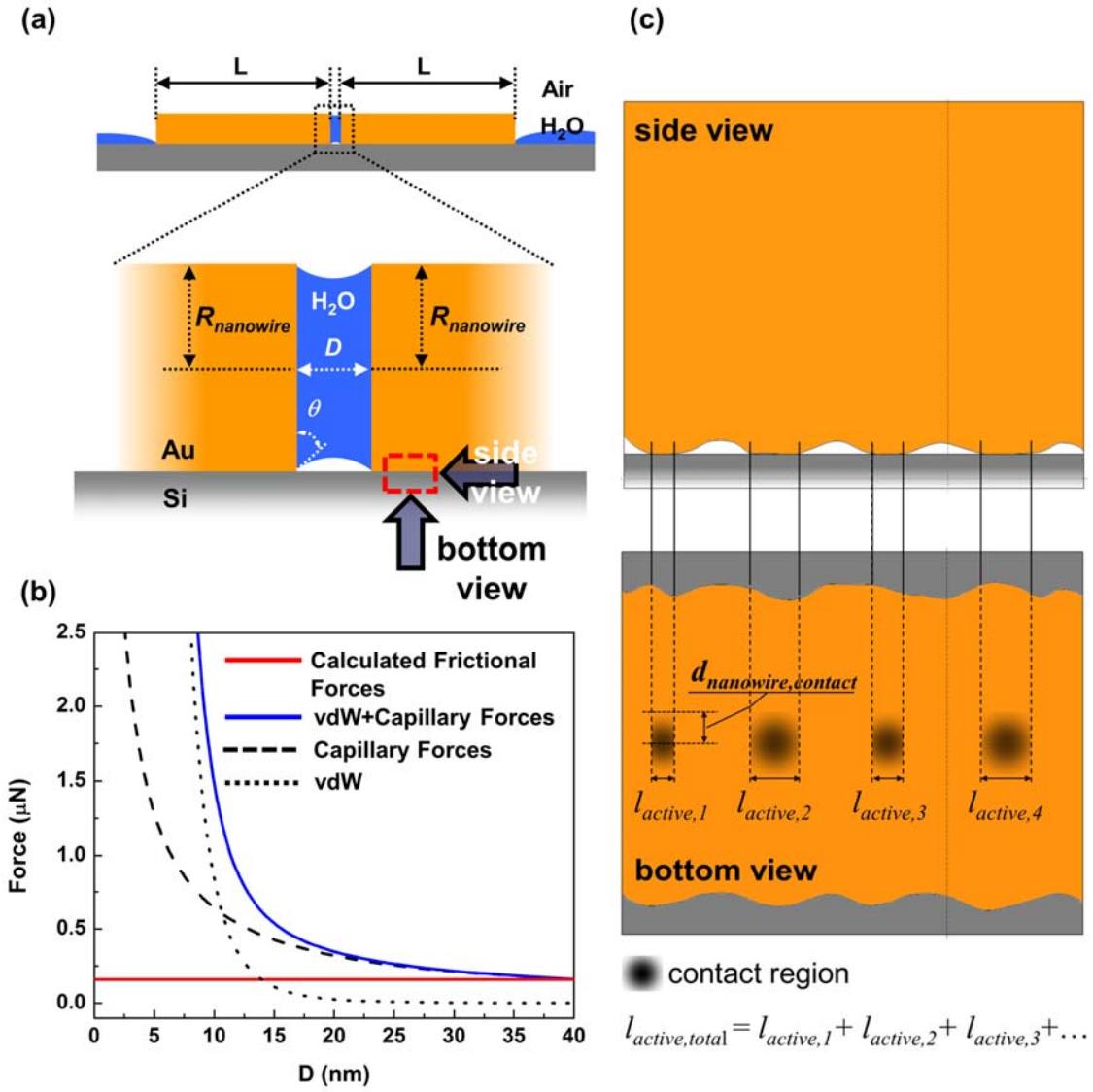

Figure 2. (a) Model of the self-contacting junctions and the parameters used for calculating attractive and repulsive forces. (b) Capillary forces (dashed black line) act at larger distances, while van der Waals

forces (dotted black line) are the dominant forces at shorter distances. Two Au segments can be brought into contact with each other when the joint effect of capillary and van der Waals forces is stronger than the frictional forces (red line) acting against movement of the Au segments on the substrate. (c) An aerial view (top) and a close up (middle, and bottom) of the boxed region of panel (a).

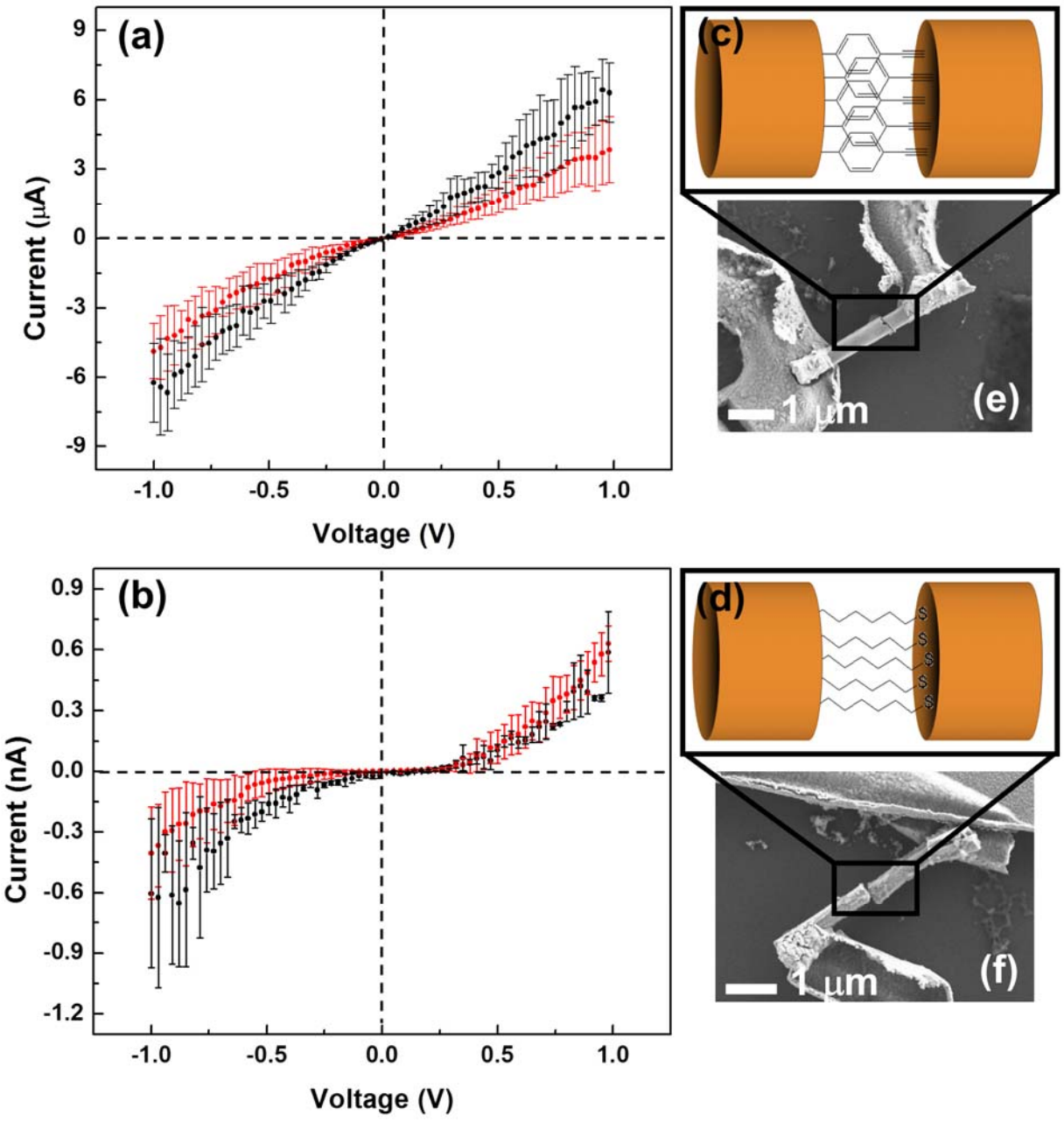

Figure 3. (a), (b) *I–V* curves of (c) 1,4-diethynyl benzene and (d) 1,6-hexanedithiol measured at 760 Torr (black) or 6×10^{-6} Torr (red). SEM images of MTJs are shown in (e) and (f).

Molecular transport junctions (MTJs) are important components in molecular electronic devices. However, the synthesis of MTJs remains a significant challenge, as the dimensions of the junction must be tailored for each experiment, based on the molecular lengths. Herein, we report a novel methodology for forming MTJs, taking advantage of capillary and van der Waals forces.

Keyword: molecular transport junction, on-wire lithography, molecular electronics, DLVO theory

Jong Kuk Lim,[1] Sarah Hurst Petrosko,[2,3] One-Sun Lee,[4] Jae-Won Jang,[5] George C. Schatz,[2,6] and Chad A. Mirkin[2,3,7]**

Molecular Transport Junctions Created By Self-Contacting Gapped Nanowires Prepared via On-Wire Lithography

Supporting Information

Molecular Transport Junctions Created By Self-Contacting Gapped Nanowires Prepared via On-Wire Lithography

Jong Kuk Lim,[1] Sarah Hurst Petrosko,[2,3] One-Sun Lee,[4] Jae-Won Jang,[5] George C. Schatz,[2,6] and Chad A. Mirkin[2,3,7]**

1. Capillary force

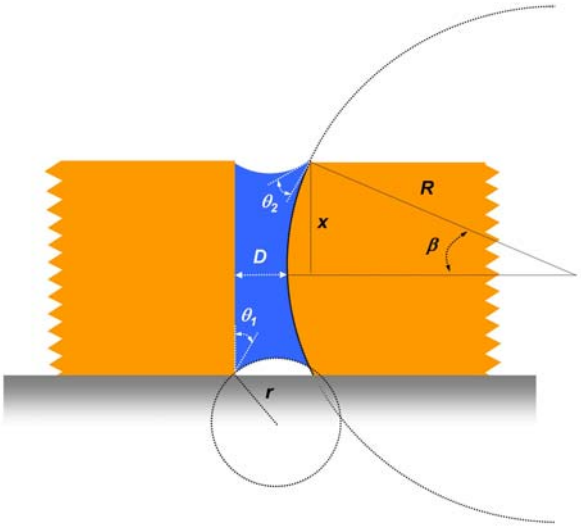

Figure S1. Capillary force acting between sphere and plane.

In Figure S1, the capillary force is given by Equation (S1)

$$F_{capillary} = \frac{\pi x^2 \gamma}{r} \quad \text{(S1)}$$

where γ is the surface tension of the liquid between the two Au segments and r is the radius of curvature of the meniscus, calculated using Equation (S2).

$$r = \frac{R(1-\cos\beta)+D}{\cos(\theta_1+\beta)+\cos\theta_2} \quad \text{(S2)}$$

Here, D is the distance from the cross-sectional surfaces of the left segment, and θ is contact angle. If R is infinitely large, we can assume that the cross-sectional surface of the right segment is not curved, but flat. Moreover, if the two segments are composed of the same materials, θ_1 equals with θ_2. For small β and $\theta_1 = \theta_2$,

$$r = \frac{D}{2\cos\theta_1} \quad \text{(S3)}$$

Finally, the capillary force, $F_{capillary}$, is

$$F_{capillary} = \frac{\pi x^2 \gamma \times 2cos\theta}{D} \quad \text{(S4)}$$

2. Frictional forces

The reduced elastic modulus, K, was calculated using Equation (S5).

$$K = \frac{4}{3}\left(\frac{\left(1-\nu_{Au}^2\right)}{E_{Au}} + \frac{\left(1-\nu_{Si_3N_4 or Si}^2\right)}{E_{Si_3N_4 or Si}}\right)^{-1} \quad \text{(S5)}$$

The Young's modulus, E, and the Poisson ratio, ν, for Au, Si_3N_4, or Si are 78.5, 140, or 160 GPa, and 0.42, 0.3, or 0.27, respectively. K is 78.5 GPa or 81.9 GPa for Au–Si_3N_4 or Au–Si, respectively.

The adhesion energy per unit area for the tip, W_{tip} is given by Equation (S6)[26]

$$W_{tip} = -\frac{F_{pull-off}}{2\pi R_{tip}} \quad \text{(S6)}$$

where $F_{pull\text{-}off,tip}$ was measured to be –23 nN, and R_{tip} is 50 nm in a previous paper.[18]

W_{tip} was calculated to be 0.073 Jm^{-2} using Equation (S7).

$$W_{tip} = -\frac{-23\times10^{-9}\ \mathrm{N}}{2\pi\times50\times10^{-9}\ \mathrm{m}} = 0.073\ \mathrm{Jm^{-2}} \quad \text{(S7)}$$

Assuming that W_{tip} is similar in value to $W_{nanowire}$, the width of the contact region for the nanowire, $d_{nanowire}$, and contact radius for the tip, r_{tip}, is given by Equations (S8) and (S9), respectively.

$$d_{nanowire,contact} = \left(\frac{2\pi\times180^2\times10^{-18}\ \mathrm{m^2}\times0.073\ \mathrm{Jm^{-2}}}{81.9\times10^{9}\ \mathrm{Nm^{-2}}}\right)^{\frac{1}{3}} = 5.7\times10^{-9}\,\mathrm{m} \quad \text{(S8)}$$

$$r_{tip,contact} = \left(\frac{2\pi\times50^2\times10^{-18}\ \mathrm{m^2}\times0.073\ \mathrm{Jm^{-2}}}{78.5\times10^{9}\ \mathrm{Nm^{-2}}}\right)^{\frac{1}{3}} = 2.4\times10^{-9}\ \mathrm{m} \quad \text{(S9)}$$

The areas of contact of the nanowire and tip, $A_{nanowire,contact}$ and $A_{tip,contact}$, were obtained using Equations (S10) and (S11), respectively.

$$A_{nanowire,contact} = 2d_{nanowire,contact}\times l_{active,total} = 11.4\ \mathrm{nm}\times l_{active,total} \quad \text{(S10)}$$

$$A_{tip,contact} = \pi\left(r_{tip,contact}\right)^2 = \pi\left(2.4\times10^{-9}\ \mathrm{m}\right)^2 = 1.8\times10^{-17}\ \mathrm{m^2} \quad \text{(S11)}$$

The frictional force measured for the tip was 0.5 nN. Assuming that the frictional force is linearly proportional to the area of contact, the frictional force for the nanowire can be calculated using Equation (S12).

$$F_{friction,nanowire} = 0.5\ \mathrm{nN}\times\frac{A_{nanowire,contact}}{A_{tip,contact}} \quad \text{(S12)}$$

The ratio of the contact area between the tip and the nanowire is given by Equation (S13)

$$\frac{A_{nanowire}}{A_{tip}} = \frac{11.4\times10^{-9}\ \mathrm{m}\times l_{active,total}}{1.8\times10^{-17}\ \mathrm{m^2}} = 6.3\times10^{8}\times l_{active,total}\ \mathrm{m^{-1}} \quad \text{(S13)}$$

where l is the effective contact length of the nanowire. Therefore, the frictional force for the nanowire is given by Equation (S14).

$$F_{friction,nanowire}\left(\mathrm{N}\right) = 0.5\times10^{-9}\ \mathrm{N}\times6.3\times10^{8}\ \mathrm{m^{-1}}\times l_{active,total}\left(\mathrm{m}\right) = 3.2\times10^{-1}\left(\mathrm{N/m}\right)\times l_{active,total}\left(\mathrm{m}\right) \quad \text{(S14)}$$

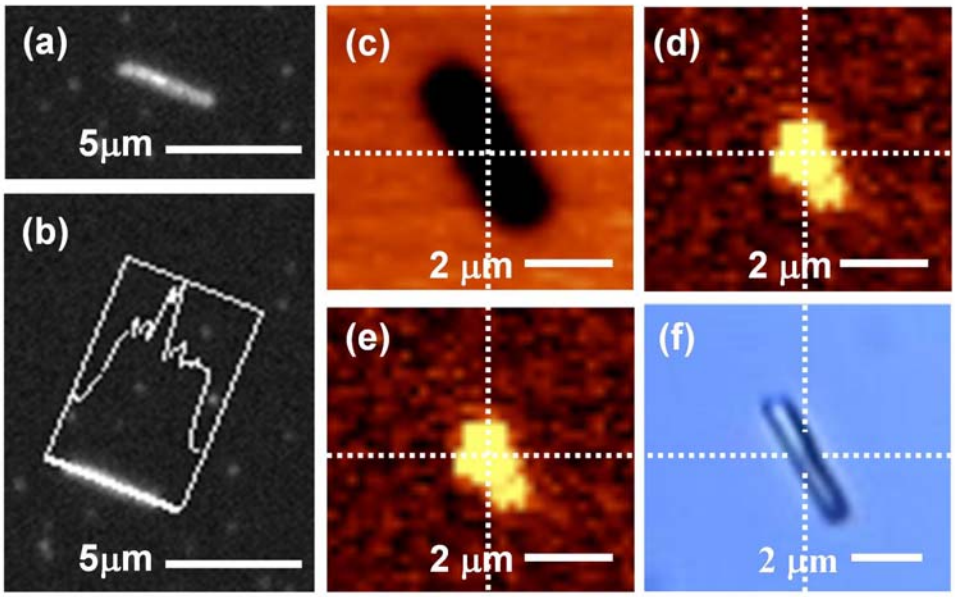

Figure S2. (a) A dark-field fluorescence optical micrograph of a self-contacting junction with fluorescein adsorbed in the junction. (b) Intensity profile of Figure S2a, showing that the fluorescence is strongest in the middle of the nanowire, which demonstrates that fluorescein is adsorbed in the junction. (c, d, and e) Confocal scanning Raman microscopy images of self-contacting junctions prepared with methylene blue in the gap. Raman images filtered with a unique Raman band from (Figure S2c) the Si wafer (520 cm^{-1}) and (Figures S2d and S2e) methylene blue (1620 cm^{-1}). (f) The corresponding bright-field optical micrograph that shows where the particle junction is located.

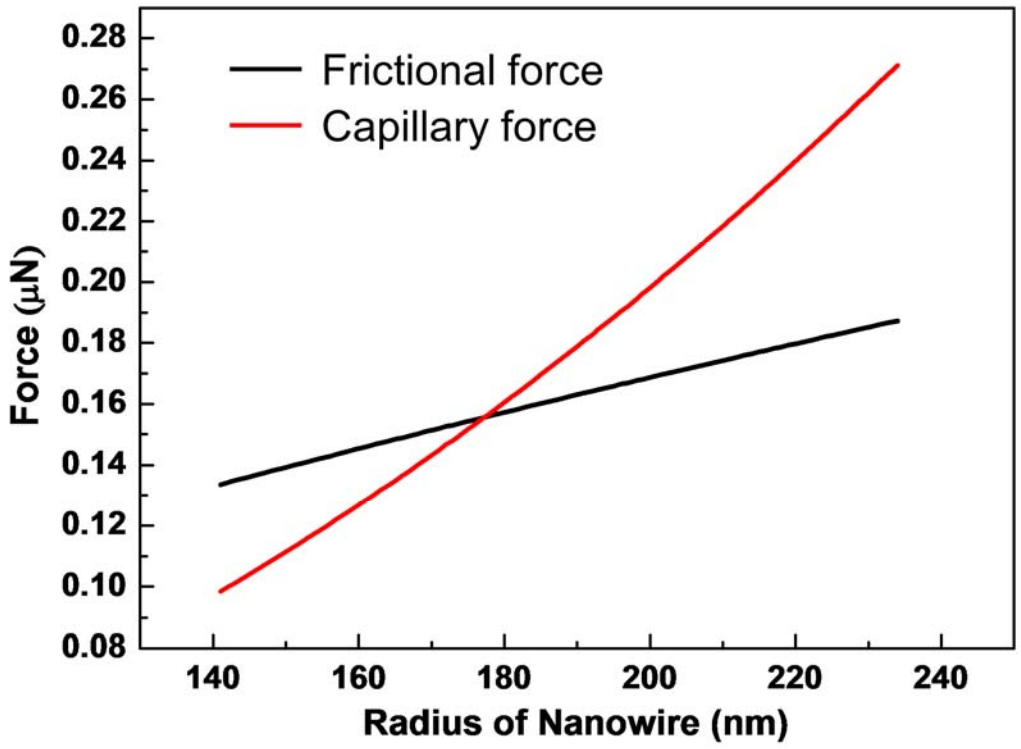

Figure S3. Frictional ($F_{friction,nanowire}$) and capillary ($F_{capillary}$) forces were calculated for nanowires of different radii (ranging from 140 - 230 nm), $R_{nanowire}$, with a fixed total active length ($l_{active,total} \approx 500$ nm), and these values were plotted against the nanowire radius. As $R_{nanowire}$ increases, both frictional and capillary forces become stronger at different rates. When $R_{nanowire}$ reaches ~180 nm, the frictional force should be similar to the capillary force. This was expected, because $l_{active,total}$ was adjusted so that $F_{friction,nanowire}$ and $F_{capillary}$ were similar at that distance. When $R_{nanowire} >$ ~180 nm, $F_{capillary}$ becomes stronger than $F_{friction,nanowire}$; the opposite happens when $R_{nanowire} <$ ~180 nm. This means that the occurrence of self-contact is easy ($R_{nanowire} >$ ~180 nm) or difficult ($R_{nanowire} <$ ~180 nm), depending on $R_{nanowire}$.